

Article

Charge Transport in Sequence-Defined Conjugated Oligomers

Hao Yu, Songsong Li, Kenneth E. Schwieter, Yun Liu, Boran Sun, Jeffrey S. Moore, and Charles M. Schroeder

J. Am. Chem. Soc., **Just Accepted Manuscript** • DOI: 10.1021/jacs.0c00043 • Publication Date (Web): 18 Feb 2020

Downloaded from pubs.acs.org on February 18, 2020

Just Accepted

“Just Accepted” manuscripts have been peer-reviewed and accepted for publication. They are posted online prior to technical editing, formatting for publication and author proofing. The American Chemical Society provides “Just Accepted” as a service to the research community to expedite the dissemination of scientific material as soon as possible after acceptance. “Just Accepted” manuscripts appear in full in PDF format accompanied by an HTML abstract. “Just Accepted” manuscripts have been fully peer reviewed, but should not be considered the official version of record. They are citable by the Digital Object Identifier (DOI®). “Just Accepted” is an optional service offered to authors. Therefore, the “Just Accepted” Web site may not include all articles that will be published in the journal. After a manuscript is technically edited and formatted, it will be removed from the “Just Accepted” Web site and published as an ASAP article. Note that technical editing may introduce minor changes to the manuscript text and/or graphics which could affect content, and all legal disclaimers and ethical guidelines that apply to the journal pertain. ACS cannot be held responsible for errors or consequences arising from the use of information contained in these “Just Accepted” manuscripts.

Charge Transport in Sequence-Defined Conjugated Oligomers

Hao Yu^{1†}, *Songsong Li*^{2,4†}, *Kenneth E. Schwierter*³, *Yun Liu*^{3,4}, *Boran Sun*¹, *Jeffrey S. Moore*^{2,3,4},
and Charles M. Schroeder^{1,2,3,4*}

¹Department of Chemical and Biomolecular Engineering, University of Illinois at Urbana-Champaign, Urbana, Illinois 61801, United States

²Department of Materials Science and Engineering, University of Illinois at Urbana-Champaign, Urbana, Illinois 61801, United States

³Department of Chemistry, University of Illinois at Urbana-Champaign, Urbana, Illinois 61801, United States

⁴Beckman Institute for Advanced Science and Technology, University of Illinois at Urbana-Champaign, Urbana, Illinois 61801, United States

†Contributed equally to this work.

*To whom correspondence should be addressed.

Email: cms@illinois.edu

Keywords: sequence-defined oligomers, single molecule charge transport, scanning tunneling microscope break-junction (STM-BJ)

ABSTRACT

A major challenge in synthetic polymers lies in understanding how primary monomer sequence affects materials properties. In this work, we show that charge transport in single molecule junctions of conjugated oligomers critically depends on the primary sequence of monomers. A series of sequence-defined oligomers ranging from two to seven units was synthesized by an iterative approach based on the van Leusen reaction, providing conjugated oligomers with backbones consisting of para-linked phenylenes connected to oxazole, imidazole, or nitro-substituted pyrrole. The charge transport properties of these materials were characterized using a scanning tunneling microscope-break junction (STM-BJ) technique, thereby enabling direct measurement of molecular conductance for sequence-defined dimers, trimers, pentamers, and a heptamer. Our results show that oligomers with specific monomer sequences exhibit unexpected and distinct charge transport pathways that enhance molecular conductance more than 10-fold. A systematic analysis using monomer substitution patterns established that sequence-defined pentamers containing imidazole or pyrrole groups in specific locations provide molecular attachment points on the backbone to the gold electrodes, thereby giving rise to multiple conductance pathways. These findings reveal the subtle but important role of molecular structure including steric hinderance and directionality of heterocycles in determining charge transport in these molecular junctions. This work brings new understanding for designing molecular electronic components.

INTRODUCTION

Sequence-defined oligomers (SDOs) and sequence-defined polymers (SDPs) are chain molecules with a precise order of monomer units; each molecule has a monomeric sequence that is identical to every other molecule^{1,2}. Sequence definition in nucleic acids and proteins is essential to the molecular blueprint of cellular functions. In synthetic materials, SDOs and SDPs offer a new dimension to manipulate self-assembly^{3,4}, catalysis⁵, nanoelectronics⁶, molecular recognition⁷, molecular encoding of information⁸, and phase behavior in polyelectrolytes⁹. Despite many recent advances, relating primary monomer sequence to the physical, chemical, and electronic properties of organic materials remains an unsolved problem^{10,11}.

The synthetic availability of precision SDOs has hindered progress in realizing structure-function relations¹. Major challenges lie in the efficient and scalable production of non-biological oligomers and polymers with discrete chain lengths and sequences. Indeed, the efficient synthesis of non-biological SDOs and SDPs has been called a “Holy Grail” of polymer science¹². Various synthetic methods have been pursued, including iterative synthesis^{13,14}, template-based synthesis¹⁵, and controlled step- or chain-growth statistical polymerization^{6,16–19}. Recently, advanced synthesis methods and molecular designs including automated synthesis techniques^{20,21} and artificial catalytic molecular machines²² have been introduced into this burgeoning field and continue to open new avenues for the precise synthesis of sequence-defined materials. However, developing synthetic schemes that afford conjugated backbones remains a key challenge. The most useful synthetic methods would be able to draw from a variety of building blocks such as aromatic carbocyclics and heterocyclics. Such methods make possible the establishment of sequence-property correlations beginning from a discrete reference sequence followed by the addition or

1
2
3 replacement of monomers at specific locations and subsequently determining the change in
4
5 properties.
6

7
8 To date, there have been limited studies correlating sequence and properties in a ‘monomer by
9
10 monomer’ fashion. Nevertheless, pioneering works from Hawker²³, Li²⁴, Lutz²⁵, McNeil²⁶,
11
12 Meyer²⁷, Noonan²⁸, Segalman²⁹ and Zuckermann³⁰ have highlighted sequence-regulation as a
13
14 promising and powerful method to control the properties of SDOs and SDPs. In SDOs and SDPs,
15
16 each monomer contributes to the backbone’s electronic structure and functional group
17
18 placement by altering chain conformation and molecular geometry. Intrinsic monomeric
19
20 contributions to bulk materials properties are difficult to disentangle due to the contributions
21
22 from intermolecular and intramolecular factors. To this end, single molecule techniques offer
23
24 the ability to directly probe properties at the molecular scale, thereby enabling elucidation of
25
26 quantitative structure-property relationships (QSPR) for sequence-defined materials^{31,32}. Single
27
28 molecule junctions have been used to study charge transport as a function of molecular length³³,
29
30 aromaticity³⁴, anchor groups³⁵, chemical substituents³⁶, bias voltage³⁷, molecular conformation³⁸
31
32 and orbital alignment between molecular bridges and metallic electrodes³⁹. The direct
33
34 measurement of single molecule conductance provides the opportunity to probe the intrinsic
35
36 relationship between sequence and electronic properties.
37
38
39
40
41

42
43 In this work, the synthesis of precisely defined conjugated SDOs is described together with
44
45 single molecule conductance measurements and molecular simulations. We first establish an
46
47 iterative strategy for synthesizing sequence-defined conjugated oligomers using the van Leusen
48
49 heterocycle synthesis. This approach was applied to the synthesis of a series of SDOs consisting
50
51 of alternating p-phenylene and heterocyclic units. Unlike traditional iterative synthetic schemes
52
53 that require chemically distinct monomers, our approach provides sequence definition by
54
55
56
57
58
59
60

1
2
3 altering reaction conditions in each synthetic cycle using a universal monomer. Following
4
5 synthesis, we directly characterize the molecular conductance and charge transport properties
6
7 of the SDO library using a scanning tunneling microscope-break junction (STM-BJ) method.
8
9 Our results show that molecular junctions with specific monomer sequences exhibit multiple
10
11 distinct charge transport pathways, some of which enhance conductance more than 10-fold. In
12
13 tandem, we characterize the distinct conductance pathways using a series of structural
14
15 analogues in concert with molecular modeling. Our results show that the high conductance
16
17 pathways emerge from gold-molecule linkages through imidazole and nitro-substituted pyrrole
18
19 located within the oligomer backbone. In this way, geometrical effects including sequence-
20
21 controlled directionality and steric hinderance of side chains determine intramolecular charge
22
23 transport in conjugated oligomers. The role of primary monomer sequence and its role on charge
24
25 transport in molecular junctions is elucidated, which will inform the design of molecular
26
27 electronic devices.
28
29
30
31
32
33

34 RESULTS AND DISCUSSION

35 Synthetic Strategy, Preparation, and Characterization

36
37
38 An iterative approach was developed for synthesizing discrete, conjugated oligomers with
39
40 wide ranging compositions and sequence variations. Since 1972, tosylmethyl isocyanide
41
42 (TosMIC) and its aryl-substituted homologues have been widely used as a C-N=C synthon in
43
44 the synthesis of multiple heterocycles including oxazoles, imidazoles, and pyrroles, which are
45
46 collectively known as van Leusen multicomponent reactions (van Leusen MCRs)⁴⁰. Here, we
47
48 design a monomer (**M**) containing the requisite tosylmethyl isocyanide group for heterocycle
49
50 synthesis and a latent functionality (nitrile) for subsequent additions by reductive conversion to
51
52 a terminal aldehyde. The iterative method consists of two steps (**Fig. 1a**): (1) a coupling reaction,
53
54
55
56
57
58
59
60

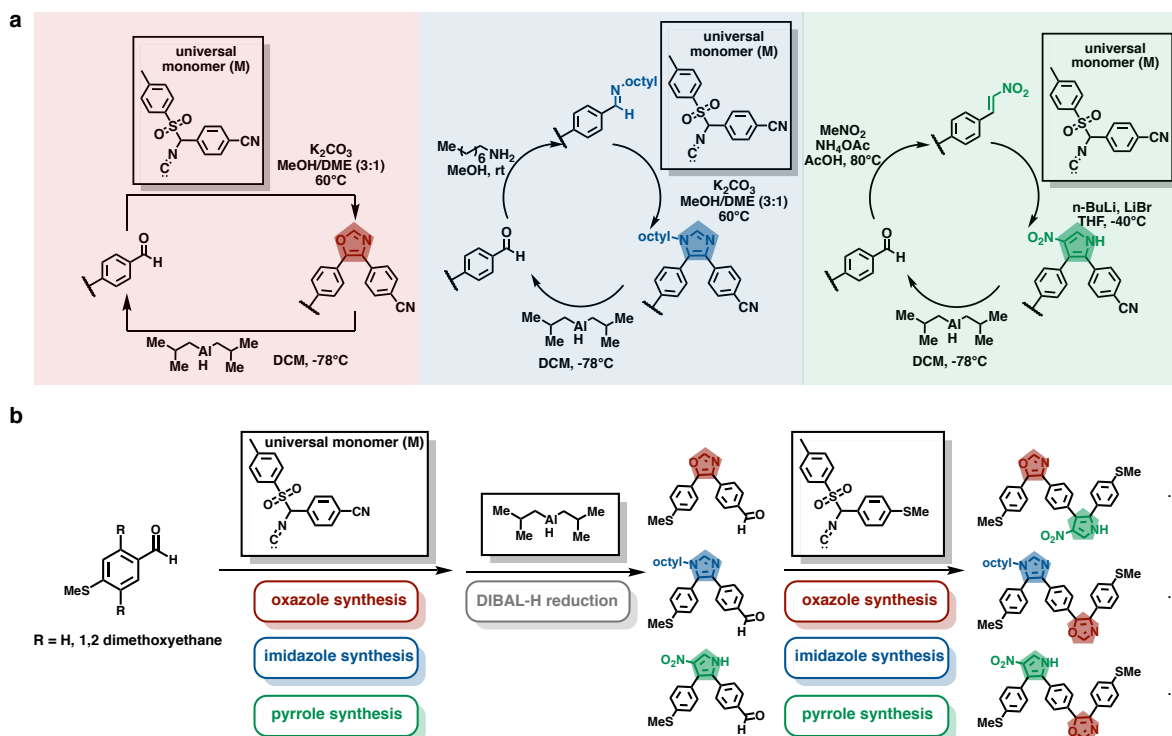


Figure 1. Iterative Synthesis of Sequence-Defined Oligomers.

(a) Iterative approach consisting of a coupling reaction and a subsequent reduction for the synthesis of alternating para-substituted phenyls linked to oxazole, imidazole, or nitro-substituted pyrrole.

(b) Schematic of sequence-controlled synthesis for pentamers. Three different heterocycles (oxazole, imidazole, or nitro-substituted pyrrole) are generated by varying the reaction conditions in each cycle to achieve sequence-defined oligomers. Oligomers are terminated with methyl sulfide to facilitate single molecule conductance measurements.

which is used to generate a heterocycle (oxazole, imidazole, or nitro-substituted pyrrole) from an aldehyde by proceeding through one of three homologous van Leusen MCRs, and (2) a reduction, which returns an aldehyde from the terminal nitrile using diisobutylaluminum hydride (DIBAL-H), thereby enabling additional coupling reactions in subsequent steps. Oligomers prepared by this approach have an ortho connectivity to the heterocycle, which leads to a twisting between the phenylene and heterocycle in the molecular backbone. Additional diversity was achieved by including chemical substitutions such as 1,2-dimethoxyethane on the phenylene group. Broadly speaking, this strategy allows for preparation of compositionally rich sequences of defined length with a limited set of building blocks.

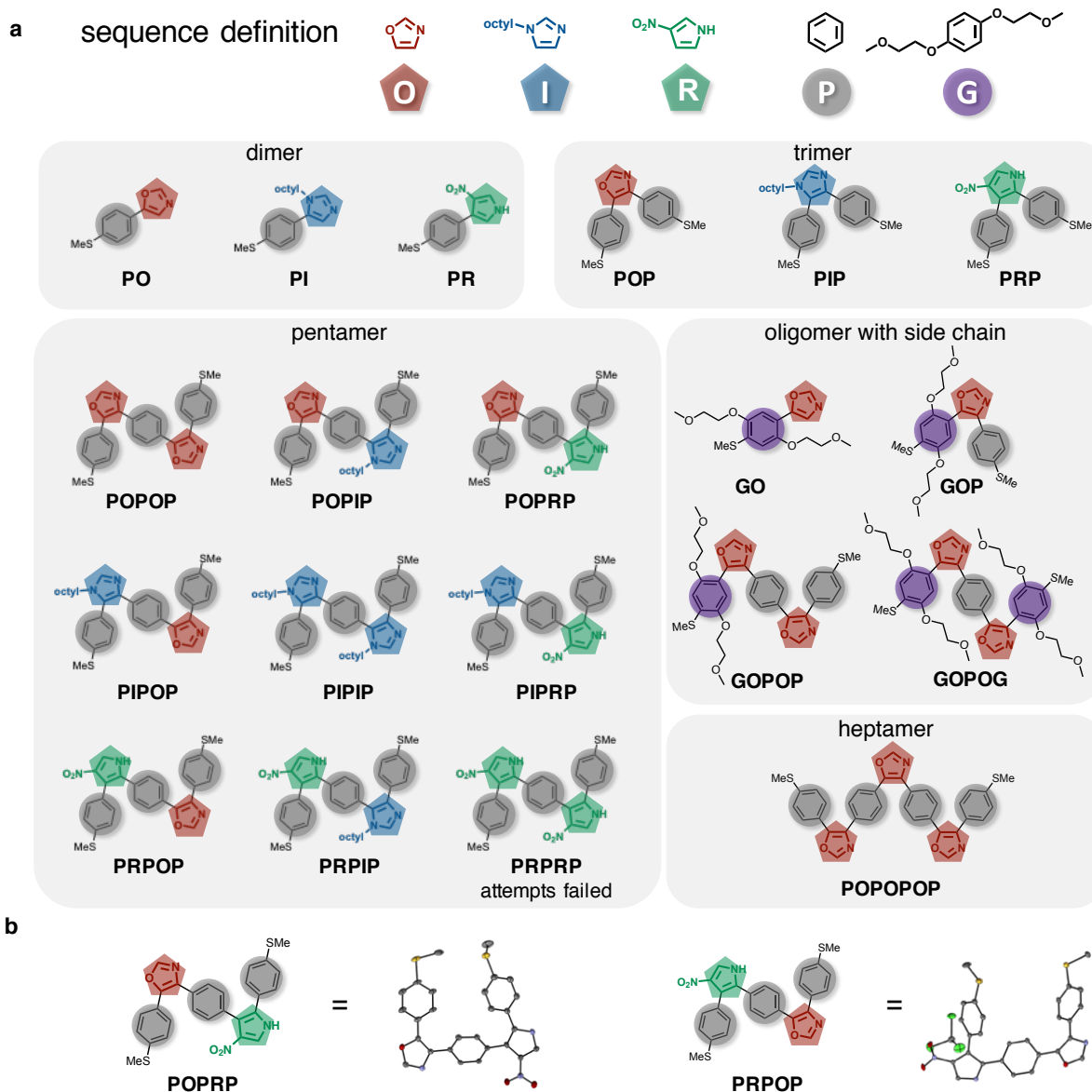


Figure 2. Sequence-Defined Conjugated Oligomers with Alternating Phenyl Heterocycle Backbones.

(a) Building blocks for sequence definition, O (oxazole), I (imidazole), R (pyrrole), P (phenyl), and G (substituted phenyl). Molecular library of sequence-defined dimers, trimers, pentamers, and heptamer.

(b) Crystal structures of **POPRP** and **PRPOP** formed by slow evaporation from a mixed solvent (chloroform/*n*-hexane). Hydrogen atoms are removed for clarity, and a CHCl_3 molecule is located within the unit cell of **PRPOP**.

Using the iterative approach described above, 19 SDOs were prepared ranging in length from dimer to heptamer (**Fig. 2a**). In particular, we synthesized nearly all possible dimeric, trimeric, and pentameric sequences with unsubstituted phenylene units. Attempts to synthesize the

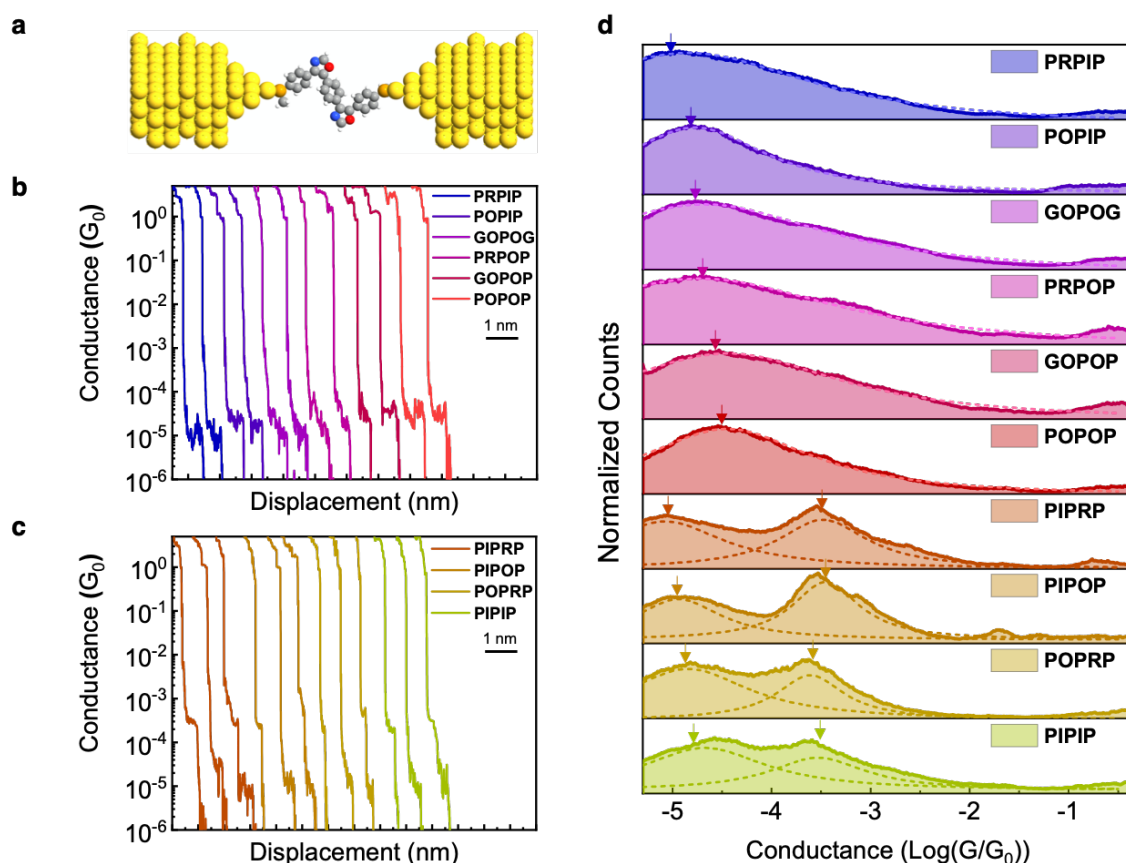


Figure 3. Single Molecule Conductance of Sequence-Defined Oligomers.

(a) Schematic illustration of single molecule break junction.

(b) Characteristic single molecule conductance traces of sequence-defined pentamers showing a single conductance peak (applied bias 0.25 V).

(c) Characteristic single molecule conductance traces of sequence-defined pentamers exhibiting multiple conductance peaks (applied bias 0.25 V). For these oligomers, two well-spaced conductance peaks are observed (high conductance $10^{-3.5} G_0$, low conductance 10^{-4} - $10^{-5} G_0$).

(d) Series of 1D conductance histograms for 10 sequence-defined pentamers (applied bias 0.25 V). Some sequences exhibit multiple conductance peaks associated with multiple molecular conductance pathways. Dotted line shows the result of Lorentzian fitting.

pentamer containing two pyrrole units failed, presumably because of side reactions between the pyrrole-containing precursor and the reagent *n*-butyllithium in the second iterative cycle. Broadly speaking, this methodology is generalizable to synthesize oligomers beyond the heptameric length and the sequence variations described here.

1
2
3 The structure of each SDO was confirmed by ^1H and ^{13}C NMR spectroscopy and mass
4 spectrometry (Supporting Information, **Sections 1-3** and **Figs. S1-S80**). Sequence-defined
5 oligomers are referred to using a naming convention based on the substituent building blocks
6 (**Fig. 2**). Pentamers containing the same composition but with different sequences are
7 structurally distinct. For example, **PIPOP** and **POPIP** are constitutional isomers with different
8 heterocycle directionalities that may impact charge transport, as discussed below. A pair of
9 isomeric pentamers, **POPRP** and **PRPOP**, crystallized as slender prisms under ambient
10 conditions. Single-crystal X-ray diffraction analysis reveal that both oligomers have similar
11 twisted U-shaped conformations in the solid state (**Fig. 2b**). Interestingly, primary sequence
12 also plays an important role in solid state structures such that **POPRP** and **PRPOP** have
13 different packing patterns (Supporting Information, **Figs. S81-S84**). By using different
14 solutions as mixed solvents (chloroform/*n*-hexane or ethyl acetate/*n*-hexane), we also observed
15 two polymorphs of **POPRP** (Supporting Information, **Tables S1-S2** and **Figs. S81-S82**) and
16 one solvatomorph of **PRPOP** (Supporting Information, **Tables S3-S4** and **Figs. S83-S84**).

36 **Single Molecule Conductance of Sequence-Defined Oligomers**

37
38 We employed a single molecule measurement - electronic conductance - to directly measure
39 the charge transport properties of each SDO. In particular, molecular conductance is determined
40 using a scanning tunneling microscope-break junction (STM-BJ) technique as previously
41 described (**Fig. 3a** and Supporting Information, **Sections 5** and **Figs. S85-S105**)^{29,41}. In all cases,
42 experiments are repeated on at least 10^3 - 10^4 individual molecules using the STM-BJ technique to
43 enable robust statistical analysis. The SDOs contain dual terminal methyl sulfide (-SMe) groups
44 that serve as anchors for making robust connections to gold electrodes^{33,41,43}. Individual
45 molecular conductance traces (**Figs. 3b, 3c**) are compiled into one-dimensional (1D) histograms
46
47
48
49
50
51
52
53
54
55
56
57
58
59
60

1
2
3 without data selection (**Fig. 3d**). In this way, 1D conductance histograms enable determination of
4 the average molecular conductance by fitting the histogrammed data to a Lorentzian function⁴⁴.
5
6 For the alternating phenylene-heterocycle oligomers in this work, we generally observe an average
7
8 molecular conductance in the range between $\sim 10^{-3}$ - $10^{-5} G_0$ (**Tables S5-S7**), where $G_0 = 77.5 \mu\text{S}$ is
9
10 the quantum unit of conductance. The ortho connectivity around heterocycles leads to a twisting
11
12 between the heterocycle and phenylene, which slightly lowers the molecular conductance
13
14 compared to fully planar structures, such as oligothiophene.³³
15
16
17
18

19 Molecular conductance in the pentamer series shows a remarkable sequence-dependent
20
21 behavior. For example, conductance histograms of two compositionally identical pentamers
22
23 **POPIP** and **PIPOP** are markedly different (**Figs. S86, S89, and S93**), such that **POPIP** shows a
24
25 predominant single peak at low conductance whereas **PIPOP** exhibits two well-spaced peaks in
26
27 molecular conductance (**Fig. 3d**). We observed two dominant and well-spaced conductance peaks
28
29 (high G and low G) in pentamers with sequences - **PIPRP, PIPOP, POPRP, and PIPIP** (**Figs. 3c,**
30
31 **3d, and S86**). Specifically, the conductance of the high G state ($10^{-3.5} G_0$) is more than one order
32
33 magnitude larger than the corresponding low G state (10^{-4} - $10^{-5} G_0$) for this set of pentamers. On
34
35 the other hand, a different set of pentamers (**PRPIP, POPRP, GOPOG, PRPOP, GOPOP, and**
36
37 **POPOP**) exhibits a primary conductance peak around 10^{-4} - $10^{-5} G_0$ and a possible obscured or
38
39 weak shoulder at a higher molecular conductance around $10^{-3.5} G_0$. To quantitatively characterize
40
41 this behavior, we used a Lorentzian fitting method to determine the relative dominance or ratio of
42
43 the primary conductance peak to possible shoulders or obscured peaks (Supporting Information,
44
45 **Sections 5.4, Fig. S106-S111**). Our results show that the pentamers **PRPIP, POPIP, GOPOG,**
46
47 **PRPOP, GOPOP, and POPOP** are well described by a primary conductance peak, which
48
49 suggests that charge transport primarily occurs through a single dominant molecular conductance
50
51
52
53
54
55
56
57
58
59
60

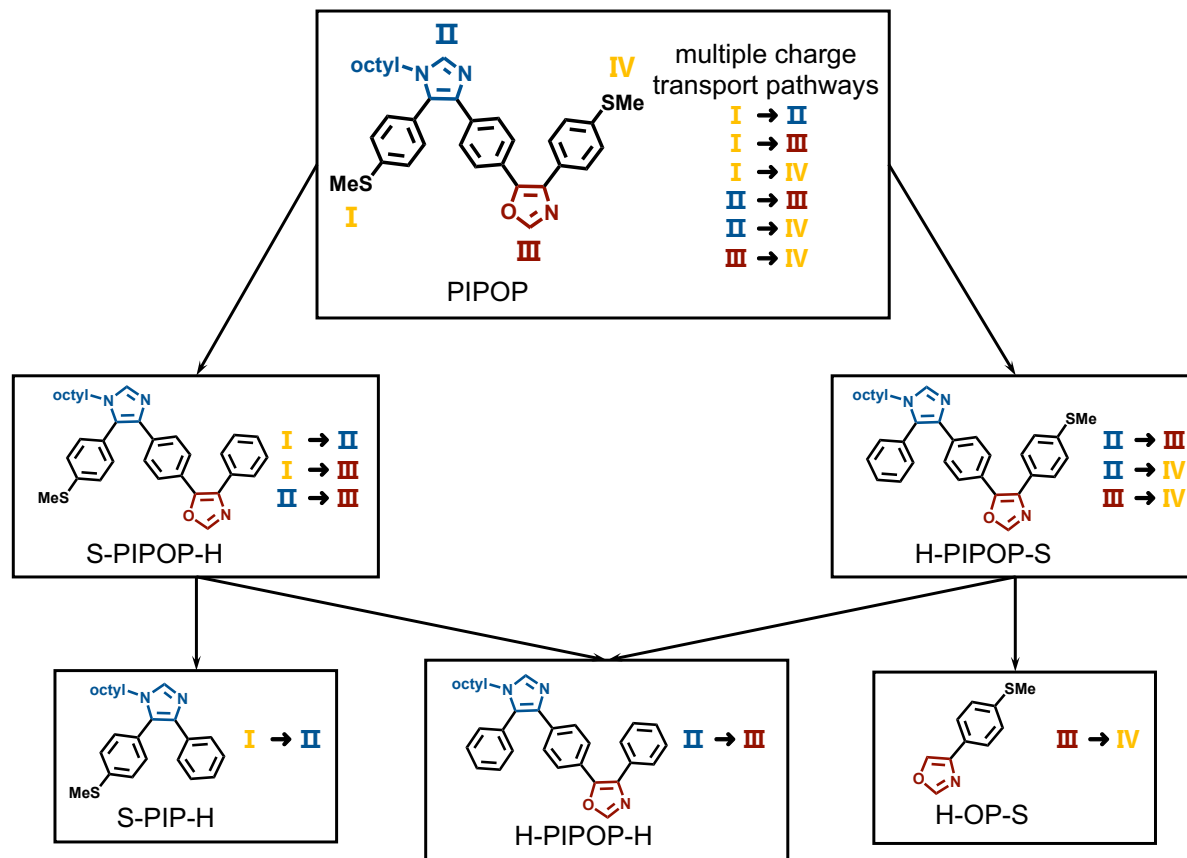


Figure 4. Structural Deconstruction to Determine Conductance Pathways. The pentamer **PIPOP** has six possible charge transport pathways corresponding to conductance from the terminal anchors and/or intramolecular heterocycles. Here, we synthesized five control compounds with lower structural complexity providing suitable models to understand the conductance pathway of the pentamer. In this way, the compounds **H-PIPOP-H**, **S-PIP-H**, and **H-OP-S** only contain a single well-defined conductive pathway.

state. Together, these results imply that the charge transport pathway in the pentamer series is dependent on primary sequence. Finally, molecular conductance results for trimers (**POP**, **PIP**, **PRP**, and **GOP**) and a heptamer (**POPOPOP**) with heterocycles located in the backbone generally show 1D conductance histograms with a single statistical conductance value (**Figs. S85, S86, and S99**).

Identifying Sequence-Controlled Conductance Pathways

Compositional variations among the 19 SDOs introduce multiple conductance pathways owing to the possibility that internal heterocycles provide anchor points between the conducting molecule

1
2
3 and the gold electrodes. In particular, the nitro group in pyrrole **R** is known to serve as a dative
4 anchor for making robust linkages to gold electrodes^{45,46}. Recent work has shown that oxazole **O**
5 serves as an efficient chemical anchor to gold electrodes for single molecule electronics⁴⁷, and the
6 imidazole **I** has a free lone electron pair on the nitrogen atom that can potentially serve as an
7 in-backbone anchoring site to gold electrodes^{48,49}.

8
9
10 A systematic structural deconstruction method was used to identify the charge transport
11 pathways of distinct conductance in the pentameric SDOs. We began by focusing on the
12 pentamer **PIPOP** and systematically examined a series of related fragments including **H-OP-S**
13 (dimer), **S-PIP-H** (trimer lacking thiomethyl anchor on one terminus), **S-PIPOP-H** (pentamer
14 lacking thiomethyl anchor on one terminus), **H-PIPOP-S** (pentamer lacking thiomethyl anchor on
15 one terminus), and **H-PIPOP-H** (pentamer lacking thiomethyl anchor on both termini) (**Fig. 4**).
16 These lower structural complexity analogs of **PIPOP** generally consist of sub-segments of the
17 pentamer or molecules lacking terminal thiomethyl anchors. In this way, the charge transport
18 pathways in these short molecular analogs are well-defined, which provides a logical and
19 systematic approach to experimentally deconstruct conductance pathways in pentamers of varying
20 sequence.

21
22
23
24
25
26
27
28
29
30
31
32
33
34
35
36
37
38
39
40
41
42
43
44
45
46
47
48
49
50
51
52
53
54
55
56
57
58
59
60
The molecular conductance of the parent pentamer and its simpler analogs were further
analyzed using two-dimensional (2D) histograms of conductance versus displacement. Prior STM-
BJ measurements have shown that the maximum displacement between the tip and substrate at
which finite conductance is measured is strongly correlated with the contour length of the
molecular junction^{50,51}. As shown in **Fig. 5a**, the 2D conductance histograms for the pentamer
PIPOP show that the high G conductance state is associated with a small tip-to-substrate
displacement of ca. 0.4 nm, whereas the low G conductance state occurs with larger molecular

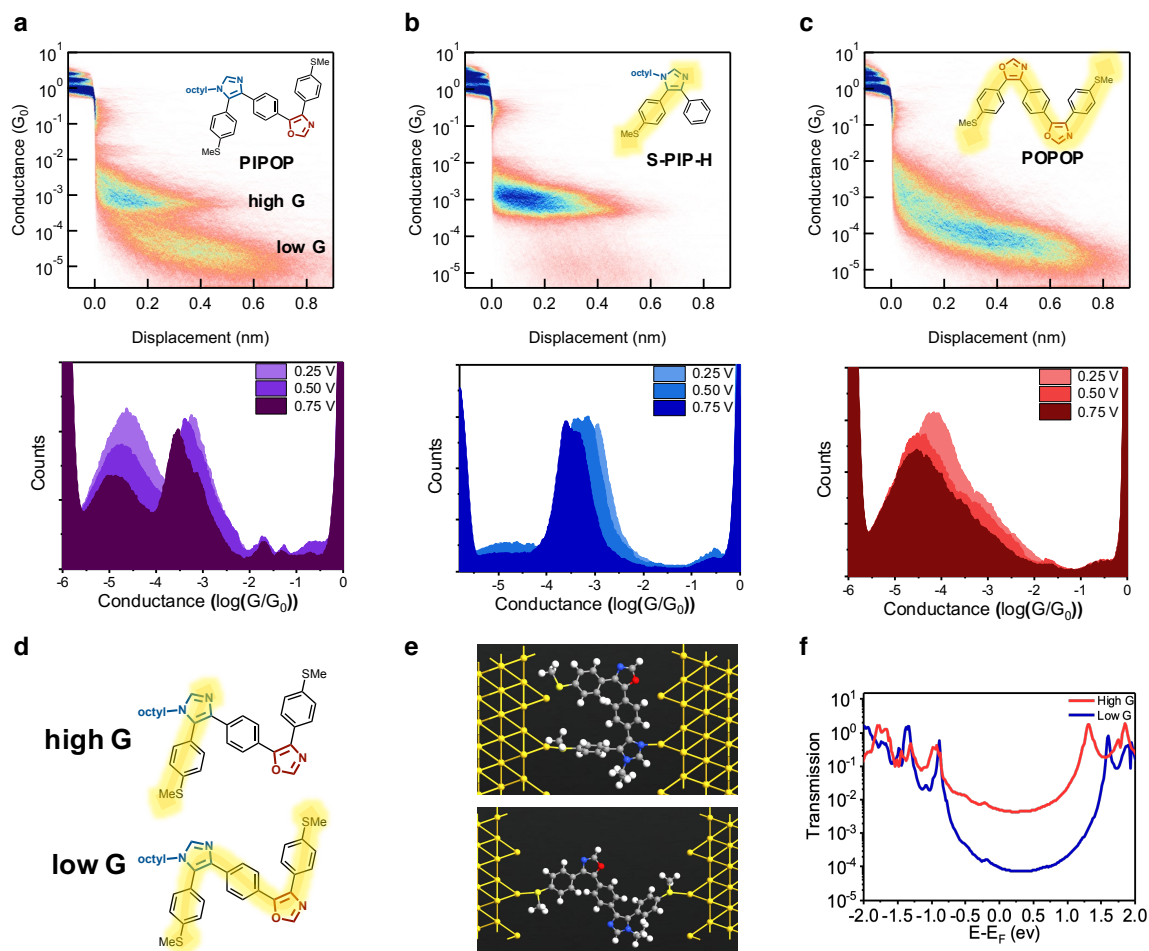


Figure 5. Molecular Conductance Pathways in Sequence-Defined Pentamers.

2D (top) conductance histograms at 0.75 V applied bias and 1D (bottom) conductance histograms (at 0.25 V, 0.50 V and 0.75 V) of (a) **PIPOP**; (b) **S-PIP-H**; and (c), **POPOP**.

(d) Mechanism for high conductance (high G) and low conductance (low G) pathways for **PIPOP**.

(e) Molecular conformations for single molecule junctions in NEGF-DFT simulations for determining transmission spectra for two distinct conductance pathways for **PIPOP**.

(f) Transmission probabilities of two distinct conductance pathways of **PIPOP** from NEGF-DFT simulations.

extensions of ca. 0.6 nm. This observation suggests that the high G state is associated with charge transport through shorter segments of the pentamer compared to the low G state.

To understand the high G charge transport pathway of the pentamer **PIPOP**, we began by characterizing the molecular conductance of **S-PIP-H** (Figs. 5b and S101), which has a defined charge transport pathway through the terminal thiomethyl anchor and the internal imidazole. Our results show that **S-PIP-H** exhibits a molecular conductance that is consistent with the high G state

1
2
3 of **PIPOP** (**Fig. 5a**) both in displacement and magnitude, across a wide range of applied bias (0.25
4 V, 0.50 V and 0.75 V) (**Figs. S89, 101**). These results are consistent with conductance in the dimer
5
6 **PI** (**Fig. S87c**) and likely arise by attaching the backbone to the gold electrode with terminal
7
8 thiomethyl anchor on one end and the central imidazole on the other. Moreover, the structural
9
10 analog **S-PIPOP-H** (**Fig. S100**) exhibits a similar high G conductance state as **S-PIP-H** (**Fig.**
11
12 **S101**), which is again attributed to charge transport through in-backbone imidazole linkages.
13
14 Interestingly, none of the other simpler analogs of **PIPOP** show a high G conductance state
15
16 observed in the parent pentamer **PIPOP** (**Figs. S102** and **S103**). Taken together, these results
17
18 strongly suggest that the high G conductance pathway of **PIPOP** arises from charge transport
19
20 through the terminal thiomethyl anchor and the internal imidazole.
21
22
23
24
25

26 Next, we analyzed the monothiolated control compounds **S-PIP-H**, **S-PIPOP-H**, and **H-**
27
28 **PIPOP-S** to reveal the nature of the low G charge transport pathway. We found that these
29
30 compounds generally exhibit conductance over a maximum displacement of ca. 0.4-0.5 nm (**Figs.**
31
32 **S100-S102**), whereas the low G state of **PIPOP** exhibits a molecular extension above 0.6 nm (**Fig.**
33
34 **5a**). Moreover, control compounds **S-PIP-H** and **S-PIPOP-H** only exhibit the high G state
35
36 consistent with **PIPOP**. On the other hand, the molecular conductance and displacement of the
37
38 low G state of **PIPOP** is consistent with pentamers that show a single conductance pathway such
39
40 as **POPOP** (**Figs. 5c, S93-S98**). Together, these results suggest that the low G conductance state
41
42 is associated with a charge transport pathway through the two terminal methyl sulfide anchors.
43
44 These results are in agreement with prior work by Gonzalez⁴⁹ and Lu⁵², where the end-to-end
45
46 molecular charge transport pathway was generally found to exhibit a lower conductance compared
47
48 to in-backbone charge transport. Our findings are summarized in a schematic in **Fig. 5d** that shows
49
50 the observed charge transport pathways for the pentamer **PIPOP**.
51
52
53
54
55
56
57
58
59
60

Molecular Origin of Sequence-Controlled Conductance Pathways

Molecular modeling using nonequilibrium Green's function-density functional theory (NEGF-DFT) is a useful way to understand charge transport pathways in sequence-defined oligomers. In all cases, molecular geometries are optimized using DFT calculations performed on Spartan'16 Parallel Suite using the B3LYP functional with a 6-31G (d,p) basis set, followed by determination of transmission functions for relaxed molecules via the Atomistix Toolkit package (**Fig. 5e**). NEGF-DFT simulations show that molecular conductance through in-backbone imidazole linkages is >10x larger than conductance through the entire end-to-end molecular contour (**Fig. 5f**). These results are consistent with the experimental results based on simpler control compounds derived from the reference pentamer.

We excluded the possibility that the high G conductance state arises from multipodal linkages between the oligomers and the gold tip and substrate. For example, it has been observed that 1,2-disilaacenaphthenes⁵¹ exhibit a relatively high conductance state arising due to multipodal linkages between the molecule and electrode surface. However, in our control experiments, the high G conductance state is observed in **S-PIP-H**, which only has two anchors including the central imidazole and terminal methyl sulfide. These results strongly suggest that the multipodal linkage mechanism is likely not observed in the phenylene heterocycle oligomers in this work.

Prior work has also shown that transient molecular conformations leads to a switching of conductance states in oligosilanes⁵³ and oligogermanes⁵⁴; however, this potential mechanism is not observed in our molecular library. DFT calculations show that the majority of pentamers have two conformations in solution: (1) a Z-shaped conformation, where the molecular backbone has a zig-zag geometry, and (2) a U-shaped conformation, where the oligomer backbone has a hairpin shape (**Fig. S112-S121**). In particular, we found that the 1,2-dimethoxyethane side chain has a

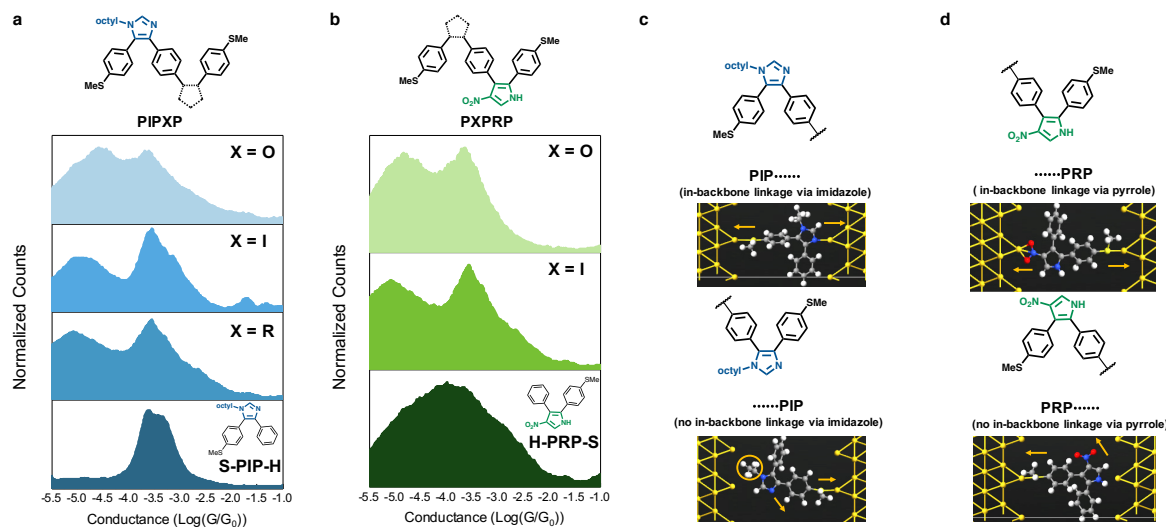


Figure 6. The Effect of Sequence on Charge Transport in Molecular Junctions.

(a) Comparison of control compound **S-PIP-H** with pentamers containing the general sequence **PIPXP** (where **X** represents an arbitrary heterocycle such as oxazole, imidazole, or nitro-substituted pyrrole) at 0.25 V.

(b) Comparison of control compound **H-PRP-S** with pentamers containing the general sequence **PXPRP** sequence at 0.25 V.

(c) Geometrical evaluation of imidazole at different positions from NEGF-DFT simulations.

(d) Geometrical evaluation of pyrrole at different positions from NEGF-DFT simulations. The directionality of **PIPXP** and **PXPRP** facilitates in-backbone linkages through imidazole or nitro-substituted pyrrole, thereby leading to a high G state. However, in-backbone linkages (high G) for **PXPIP** and **PRPXP** are inhibited due to unfavorable geometries and steric hinderance effects.

strong influence on the ratio of the Z-shaped conformation versus U-shaped conformation. For example, the Z/U conformational ratio of **POPOP**, **GOPOP**, and **GOPOG** gradually decreases from 2:1 to 0:1, such that **GOPOG** exclusively adopts the U-shaped geometry. Overall, our results show that these different molecular conformations generally exhibit similar conductance states.

We next considered the high G conductance states of the pentamer subset consisting of molecules **PIPOP**, **PIPIP**, **PIPRP**, and **POPRP**. The high G conductance states of **PIPOP**, **PIPIP**, and **PIPRP** are consistent with control compound **S-PIP-H** both in displacement and magnitude under different applied biases (0.25 V, 0.50 V and 0.75 V) (Figs. 6a, S89-91). This result demonstrates that the high G conductance state of pentamers with a **PIPXP** sequence (where **X**

1
2
3 represents an arbitrary heterocycle such as oxazole, imidazole, or nitro-substituted pyrrole) all
4 derive from an identical imidazole in-backbone linkage. In order to understand the nature of high
5 G conductance of pentamers with a **PXPRP** sequence (**POPRP** and **PIPRP**), we further
6 considered the oligomeric fragment **H-PRP-S** which is a trimeric structure lacking a thiomethyl
7 anchor on one terminus (**Fig. 6b**). Comparing **POPRP** and **PIPRP** with **H-PRP-S**, we attribute
8 the high G conductance state to an in-backbone linkage through the nitro-substituted pyrrole and
9 terminal methyl sulfide (**Figs. 6b, S90 and S92**). The slight difference in conductance magnitudes
10 between **POPRP**, **PIPRP**, and control compound **H-PRP-S** is likely due to differences in
11 conjugation in each molecular structure. The results are consistent across a wide range of bias
12 voltages (0.25 V, 0.50 V and 0.75 V) (**Figs. S104 and S105**). Nevertheless, we note that **PIPRP**
13 contains both imidazole and nitro-substituted pyrrole that may form in-backbone linkages, such
14 that conductance in **PIPRP** could arise due to a combination of two different in-backbone linkages.

15
16
17
18
19
20
21
22
23
24
25
26
27
28
29
30
31 To more deeply understand the molecular origins of monomer sequence on conductance,
32 we considered the effects of electrode-molecule alignment due to backbone geometry and
33 conformation, monomer orientation, and steric interactions. Interestingly, we observe dual
34 conductance peaks for **PIPOP**, **PIPRP**, and **POPRP**, but only a single conductance peak for
35 their regioisomers **POPIP**, **PRPIP**, and **PRPOP**, despite both sets of molecules having the
36 identical composition in terms of in-backbone anchor groups (**PIPOP** versus **POPIP**, **PIPRP**
37 versus **PRPIP**, and **POPRP** versus **PRPOP**). Imidazole and nitro-substituted pyrrole groups
38 link to gold electrodes by a noncovalent coordination interaction, and the donor-acceptor linkage
39 is expected to be highly orientated as reported prior literature^{43,48}. We therefore posit that the
40 alignment between in-backbone anchor sites and adjacent terminal anchoring groups is critically
41 important for forming robust in-backbone linkages. To test this hypothesis, we carried out DFT
42
43
44
45
46
47
48
49
50
51
52
53
54
55
56
57
58
59
60

1
2
3 simulations for geometrical analysis of the metal-molecule junction. Indeed, DFT results show that
4 favorable in-backbone linkages are formed in structures beginning with a **PIP** sequence (e.g.
5 **PIPXX**), which is greatly facilitated by a linear alignment between the imidazole anchor and the
6 terminal methyl sulfide in a two-electrode STM-BJ configuration (**Fig. 6c**). However, for
7 structures ending with a **PIP** sequence (e.g. **XXPIP**), a robust in-backbone linkage is not formed
8 largely because the relative angle between the terminal methyl sulfide and the second anchor site
9 is much smaller than 90 degrees. Moreover, octyl side chains on the substituted imidazole group
10 also introduce strong steric hinderance in molecular junctions, which further inhibit in-backbone
11 linkages.
12
13
14
15
16
17
18
19
20
21
22
23

24 Similar results are observed in cases where the in-backboned linkage is formed by a nitro-
25 substituted pyrrole. In particular, we observe that robust in-backbone linkages are only formed in
26 structures ending with a **PRP** sequence (e.g. **XXPRP**), wherein alignment between the in-
27 backbone anchor (nitro-substituted pyrrole) and the terminal anchor (methyl sulfide) is nearly
28 linear (**Fig. 6d**). This result is consistent with our experimental observation that only pentamers
29 with these two sequence characteristics (**PIPXX** or **XXPRP** sequence) exhibit two well-spaced
30 conductance peaks (**Figs. 6a** and **6b**). In general, we find that the alignment between the in-
31 backbone anchor and the terminal anchor is critically important in the formation of in-backbone
32 linkages.
33
34
35
36
37
38
39
40
41
42
43

44 We further note that in-backbone oxazole heterocycles generally do not form robust linkages
45 to gold electrodes in our sequence-defined oligomers. Prior work has shown that the electron-
46 donating ability of a lone electron pair is a key dominant factor for determining coupling strength⁴⁸.
47 Due to the strong electronegative character of oxygen, we posit that the nitrogen atom in oxazole
48 heterocycle has a relatively weak electron-donating ability compared to the nitrogen atom in
49
50
51
52
53
54
55
56
57
58
59
60

1
2
3 imidazole. Such concepts are also familiar from coordination chemistry; for example, the reported
4
5 basicity of oxazole ($pK_a = 0.8$ for the conjugate acid) and imidazole ($pK_a = 6.9$ for the conjugate
6
7 acid) are consistent with our conjecture⁵⁵. Overall, our results on sequence-controlled conductive
8
9 pathways are best explained in the context of geometrical directionality and local steric hinderance.
10
11 Together, these results may prove generalizable beyond the chemical structures described here and
12
13 could provide a design framework to understand sequence-effects in molecular electronics.
14
15

16 17 CONCLUSION

18
19 In summary, we have demonstrated that the charge transport pathway in conjugated SDOs
20
21 is precisely controlled by primary sequence, which mainly results from sequence-controlled
22
23 electrode-molecule alignment. Using an iterative synthetic approach, the position and
24
25 directionality of three distinct heterocycles (oxazole, imidazole, and nitro-substituted pyrrole)
26
27 are precisely controlled along π -conjugated backbones for oligomers ranging in size from
28
29 dimers, trimers, pentamers, and a heptamer. Among 19 SDOs and dozens of control compounds,
30
31 single molecule conductance measurements show that four pentamers with specific sequences
32
33 exhibit two distinct conductance pathways consisting of a high conductance state (ca. $10^{-3.5} G_0$)
34
35 and a low conductance state (ca. 10^{-4} - $10^{-5} G_0$). By extensively studying a series of structural
36
37 analogues coupled with molecular modeling and simulations, we find that the high conductance
38
39 state arises from charge transport through an in-backbone linkage of imidazole or nitro-
40
41 substituted pyrrole, whereas the low G conductance state arises from charge transport through
42
43 terminal methyl sulfide anchor groups. The insights provided from NEGF-DFT simulations
44
45 suggest that a linear metal-molecule alignment geometry and minimal steric hinderance between
46
47 the metallic electrode and side chain facilitate the in-backbone linkage through heterocycles.
48
49 Broadly speaking, the synthesis scheme developed in this work will enhance the capabilities of
50
51
52
53
54
55
56
57
58
59
60

1
2
3 preparing sequence-defined materials with controlled charge transport pathways. In addition, the
4 realization of underlying factors such as molecular geometry and steric interactions that are
5 regulated by primary sequence will enable new strategic molecular design strategies to build
6 materials with sequence-dependent properties.
7
8
9
10
11
12
13

14 **ASSOCIATED CONTENT**

15 **Supporting Information**

16
17 The Supporting Information is available free of charge on the ACS Publications website at DOI:
18
19 XXX. Description of chemical synthesis, chemical and physical characterization of oxazole-
20 terminated molecules, experimental details on STM-BJ, simulation methods, supporting text,
21 supporting figures.
22
23
24
25
26
27
28

29 **Corresponding Author**

30 cms@illinois.edu
31
32
33

34 **Author Contributions**

35 H.Y. and S.L. contributed equally to this work.
36
37

38 **Notes**

39 The authors declare no competing financial interests.
40
41
42

43 **ACKNOWLEDGEMENTS**

44 We thank Latha Venkataraman and Yaping Zang for generously providing advice in building the
45 STM-BJ instrument. We also thank Prapti Kafle and Ying Diao for useful discussions and Toby
46 Woods for X-ray diffraction analysis. This work was supported by the U.S. Department of Defense
47 by a MURI (Multi-University Research Initiative) through the Army Research Office (ARO)
48 through Award W911NF-16-1-037 to C.M.S. and J.S.M.
49
50
51
52
53
54
55
56
57
58
59
60

REFERENCES

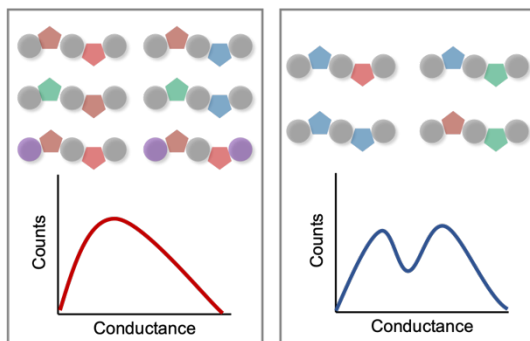
- (1) Badi, N.; Lutz, J.-F. Sequence Control in Polymer Synthesis. *Chem. Soc. Rev.* **2009**, *38* (12), 3383–3390.
- (2) Lutz, J.-F.; Ouchi, M.; Liu, D. R.; Sawamoto, M. Sequence-Controlled Polymers. *Science* (80-.). **2013**, *341* (6146).
- (3) Davidson, E. C.; M. Rosales, A.; L. Patterson, A.; Russ, B.; Yu, B.; N. Zuckermann, R.; A. Segalman, R. Impact of Helical Chain Shape in Sequence-Defined Polymers on Polypeptoid Block Copolymer Self-Assembly. *Macromolecules* **2018**, *51* (5), 2089–2098.
- (4) Epps Thomas H., I. I. I.; O'Reilly, R. K. Block Copolymers: Controlling Nanostructure to Generate Functional Materials – Synthesis, Characterization, and Engineering. *Chem. Sci.* **2016**, *7* (3), 1674–1689.
- (5) Le, D. N.; Hansen, E.; Khan, H. A.; Kim, B.; Wiest, O.; Dong, V. M. Hydrogenation Catalyst Generates Cyclic Peptide Stereocentres in Sequence. *Nat. Chem.* **2018**, *10*, 968.
- (6) Gutekunst, W. R.; Hawker, C. J. A General Approach to Sequence-Controlled Polymers Using Macrocyclic Ring Opening Metathesis Polymerization. *J. Am. Chem. Soc.* **2015**, *137* (25), 8038–8041.
- (7) Hirao, T.; Kudo, H.; Amimoto, T.; Haino, T. Sequence-Controlled Supramolecular Terpolymerization Directed by Specific Molecular Recognitions. *Nat. Commun.* **2017**, *8* (1), 634.
- (8) Lutz, J.-F. Coding Macromolecules: Inputting Information in Polymers Using Monomer-Based Alphabets. *Macromolecules* **2015**, *48* (14), 4759–4767.
- (9) Lytle, T. K.; Chang, L.-W.; Markiewicz, N.; L. Perry, S.; E. Sing, C. Designing Electrostatic Interactions via Polyelectrolyte Monomer Sequence. *ACS Cent. Sci.* **2019**, *5* (4), 709–718.
- (10) Lutz, J.-F. Defining the Field of Sequence-Controlled Polymers. *Macromol. Rapid Commun.* **2017**, *38* (24), 1700582.
- (11) Lutz, J.-F.; Ouchi, M.; Sawamoto, M.; Meyer, T. Y. Sequence-Controlled Polymers: Synthesis, Self-Assembly, and Properties. *ACS Symposium Series*. American Chemical Society January 1, 2014, p 0.
- (12) Lutz, J.-F. Sequence-Controlled Polymerizations: The next Holy Grail in Polymer Science? *Polym. Chem.* **2010**, *1* (1), 55–62.
- (13) Barnes, J. C.; Ehrlich, D. J. C.; Gao, A. X.; Leibfarth, F. A.; Jiang, Y.; Zhou, E.; Jamison, T. F.; Johnson, J. A. Iterative Exponential Growth of Stereo- and Sequence-Controlled Polymers. *Nat. Chem.* **2015**, *7*, 810.
- (14) Yang, C.; Flynn, J. P.; Niu, J. Facile Synthesis of Sequence-Regulated Synthetic Polymers Using Orthogonal SuFEx and CuAAC Click Reactions. *Angew. Chemie Int. Ed.* **2018**, *57* (49), 16194–16199.
- (15) Niu, J.; Hili, R.; Liu, D. R. Enzyme-Free Translation of DNA into Sequence-Defined Synthetic Polymers Structurally Unrelated to Nucleic Acids. *Nat. Chem.* **2013**, *5*, 282.
- (16) Pfeifer, S.; Lutz, J.-F. A Facile Procedure for Controlling Monomer Sequence Distribution in Radical Chain Polymerizations. *J. Am. Chem. Soc.* **2007**, *129* (31), 9542–9543.
- (17) Nowalk, J. A.; Fang, C.; L. Short, A.; M. Weiss, R.; H. Swisher, J.; Liu, P.; Y. Meyer, T. Sequence-Controlled Polymers Through Entropy-Driven Ring-Opening Metathesis Polymerization: Theory, Molecular Weight Control, and Monomer Design. *J. Am. Chem.*

- Soc.* **2019**, *141* (14), 5741–5752.
- (18) Kobayashi, S.; M. Pitet, L.; A. Hillmyer, M. Regio- and Stereoselective Ring-Opening Metathesis Polymerization of 3-Substituted Cyclooctenes. *J. Am. Chem. Soc.* **2011**, *133* (15), 5794–5797.
- (19) Satoh, K.; Ozawa, S.; Mizutani, M.; Nagai, K.; Kamigaito, M. Sequence-Regulated Vinyl Copolymers by Metal-Catalysed Step-Growth Radical Polymerization. *Nat. Commun.* **2010**, *1*, 6.
- (20) Li, T.; Liu, L.; Wei, N.; Yang, J.-Y.; Chapla, D. G.; Moremen, K. W.; Boons, G.-J. An Automated Platform for the Enzyme-Mediated Assembly of Complex Oligosaccharides. *Nat. Chem.* **2019**, *11* (3), 229–236.
- (21) Li, J.; Ballmer, S. G.; Gillis, E. P.; Fujii, S.; Schmidt, M. J.; Palazzolo, A. M. E.; Lehmann, J. W.; Morehouse, G. F.; Burke, M. D. Synthesis of Many Different Types of Organic Small Molecules Using One Automated Process. *Science* (80-.). **2015**, *347* (6227), 1221 LP – 1226.
- (22) Lewandowski, B.; De Bo, G.; Ward, J. W.; Pappmeyer, M.; Kuschel, S.; Aldegunde, M. J.; Gramlich, P. M. E.; Heckmann, D.; Goldup, S. M.; D'Souza, D. M.; Fernandes, A. E.; Leigh, D. A. Sequence-Specific Peptide Synthesis by an Artificial Small-Molecule Machine. *Science* (80-.). **2013**, *339* (6116), 189 LP – 193.
- (23) Lawrence, J.; Goto, E.; M. Ren, J.; McDearmon, B.; Sub Kim, D.; Ochiai, Y.; G. Clark, P.; Laitar, D.; Higashihara, T.; J. Hawker, C. A Versatile and Efficient Strategy to Discrete Conjugated Oligomers. *J. Am. Chem. Soc.* **2017**, *139* (39), 13735–13739.
- (24) Liang, L.; Wang, J.-T.; Xiang, X.; Ling, J.; Zhao, F.-G.; Li, W.-S. Influence of Moiety Sequence on the Performance of Small Molecular Photovoltaic Materials. *J. Mater. Chem. A* **2014**, *2* (37), 15396–15405.
- (25) Roy, R. K.; Lutz, J.-F. Compartmentalization of Single Polymer Chains by Stepwise Intramolecular Cross-Linking of Sequence-Controlled Macromolecules. *J. Am. Chem. Soc.* **2014**, *136* (37), 12888–12891.
- (26) F. Palermo, E.; J. McNeil, A. Impact of Copolymer Sequence on Solid-State Properties for Random, Gradient and Block Copolymers Containing Thiophene and Selenophene. *Macromolecules* **2012**, *45* (15), 5948–5955.
- (27) Zhang, S.; E. Bauer, N.; Y. Kanal, I.; You, W.; R. Hutchison, G.; Y. Meyer, T. Sequence Effects in Donor–Acceptor Oligomeric Semiconductors Comprising Benzothiadiazole and Phenylenevinylene Monomers. *Macromolecules* **2016**, *50* (1), 151–161.
- (28) Fortney, A.; Tsai, C.-H.; Banerjee, M.; Yaron, D.; Kowalewski, T.; J. T. Noonan, K. Impact of Precise Control over Microstructure in Thiophene–Selenophene Copolymers. *Macromolecules* **2018**, *51* (23), 9494–9501.
- (29) Patterson, A. L.; P. O. Danielsen, S.; Yu, B.; C. Davidson, E.; H. Fredrickson, G.; A. Segalman, R. Sequence Effects on Block Copolymer Self-Assembly through Tuning Chain Conformation and Segregation Strength Utilizing Sequence-Defined Polypeptoids. *Macromolecules* **2019**, *52* (3), 1277–1286.
- (30) Sun, J.; Liao, X.; M. Minor, A.; P. Balsara, N.; N. Zuckermann, R. Morphology-Conductivity Relationship in Crystalline and Amorphous Sequence-Defined Peptoid Block Copolymer Electrolytes. *J. Am. Chem. Soc.* **2014**, *136* (42), 14990–14997.
- (31) Xin, N.; Guan, J.; Zhou, C.; Chen, X.; Gu, C.; Li, Y.; Ratner, M. A.; Nitzan, A.; Stoddart, J. F.; Guo, X. Concepts in the Design and Engineering of Single-Molecule Electronic Devices. *Nat. Rev. Phys.* **2019**, *1* (3), 211–230.

- 1
2
3 (32) Meier, M. A. R.; Barner-Kowollik, C. A New Class of Materials: Sequence-Defined
4 Macromolecules and Their Emerging Applications. *Adv. Mater.* **2019**, *31* (26), 1806027.
- 5 (33) Capozzi, B.; Dell, E. J.; Berkelbach, T. C.; Reichman, D. R.; Venkataraman, L.; Campos,
6 L. M. Length-Dependent Conductance of Oligothiophenes. *J. Am. Chem. Soc.* **2014**, *136*
7 (29), 10486–10492.
- 8 (34) Yin, X.; Zang, Y.; Zhu, L.; Low, J. Z.; Liu, Z.-F.; Cui, J.; Neaton, J. B.; Venkataraman,
9 L.; Campos, L. M. A Reversible Single-Molecule Switch Based on Activated
10 Antiaromaticity. *Sci. Adv.* **2017**, *3* (10), eaao2615.
- 11 (35) Moreno-García, P.; Gulcur, M.; Zsolt Manrique, D.; Pope, T.; Hong, W.; Kaliginedi, V.;
12 Huang, C.; S. Batsanov, A.; R. Bryce, M.; Lambert, C.; Wandlowski, T. Single-Molecule
13 Conductance of Functionalized Oligoynes: Length Dependence and Junction Evolution. *J.*
14 *Am. Chem. Soc.* **2013**, *135* (33), 12228–12240.
- 15 (36) Zhang, N.; Lo, W.-Y.; Cai, Z.; Li, L.; Yu, L. Molecular Rectification Tuned by Through-
16 Space Gating Effect. *Nano Lett.* **2016**, *17* (1), 308–312.
- 17 (37) Bai, J.; Daaoub, A.; Sangtarash, S.; Li, X.; Tang, Y.; Zou, Q.; Sadeghi, H.; Liu, S.; Huang,
18 X.; Tan, Z.; Liu, J.; Yang, Y.; Shi, J.; Mészáros, G.; Chen, W.; Lambert, C.; Hong, W.
19 Anti-Resonance Features of Destructive Quantum Interference in Single-Molecule
20 Thiophene Junctions Achieved by Electrochemical Gating. *Nat. Mater.* **2019**, *18* (4), 364–
21 369.
- 22 (38) Aragonès, A. C.; Darwish, N.; Im, J.; Lim, B.; Choi, J.; Koo, S.; Díez-Pérez, I. Fine-
23 Tuning of Single-Molecule Conductance by Tweaking Both Electronic Structure and
24 Conformation of Side Substituents. *Chem. – A Eur. J.* **2015**, *21* (21), 7716–7720.
- 25 (39) Chen, F.; J. Tao, N. Electron Transport in Single Molecules: From Benzene to Graphene.
26 *Acc. Chem. Res.* **2009**, *42* (3), 429–438.
- 27 (40) van Leusen, A. M.; Siderius, H.; Hoogenboom, B. E.; van Leusen, D. A New and Simple
28 Synthesis of the Pyrrole Ring System from Michael Acceptors and
29 Tosylmethylisocyanides. *Tetrahedron Lett.* **1972**, *13* (52), 5337–5340.
- 30 (41) Li, B.; Yu, H.; Montoto, E. C.; Liu, Y.; Li, S.; Schwieter, K.; Rodríguez-López, J.; Moore,
31 J. S.; Schroeder, C. M. Intrachain Charge Transport through Conjugated Donor–Acceptor
32 Oligomers. *ACS Appl. Electron. Mater.* **2019**, *1* (1), 7–12.
- 33 (42) Aradhya, S. V.; Venkataraman, L. Single-Molecule Junctions beyond Electronic Transport.
34 *Nat. Nanotechnol.* **2013**, *8*, 399.
- 35 (43) Su, T. A.; Neupane, M.; Steigerwald, M. L.; Venkataraman, L.; Nuckolls, C. Chemical
36 Principles of Single-Molecule Electronics. *Nat. Rev. Mater.* **2016**, *1*, 16002.
- 37 (44) Venkataraman, L.; Klare, J. E.; Nuckolls, C.; Hybertsen, M. S.; Steigerwald, M. L.
38 Dependence of Single-Molecule Junction Conductance on Molecular Conformation.
39 *Nature* **2006**, *442* (7105), 904–907.
- 40 (45) Zotti, L. A.; Kirchner, T.; Cuevas, J.-C.; Pauly, F.; Huhn, T.; Scheer, E.; Erbe, A.
41 Revealing the Role of Anchoring Groups in the Electrical Conduction Through Single-
42 Molecule Junctions. *Small* **2010**, *6* (14), 1529–1535.
- 43 (46) Kaliginedi, V.; V. Rudnev, A.; Moreno-García, P.; Baghernejad, M.; Huang, C.; Hong,
44 W.; Wandlowski, T. Promising Anchoring Groups for Single-Molecule Conductance
45 Measurements. *Phys. Chem. Chem. Phys.* **2014**, *16* (43), 23529–23539.
- 46 (47) Li, S.; Yu, H.; Schwieter, K.; Chen, K.; Li, B.; Liu, Y.; S. Moore, J.; M. Schroeder, C.
47 Charge Transport and Quantum Interference Effects in Oxazole-Terminated Conjugated
48 Oligomers. *J. Am. Chem. Soc.* **2019**, *141* (40), 16079–16084.
- 49
50
51
52
53
54
55
56
57
58
59
60

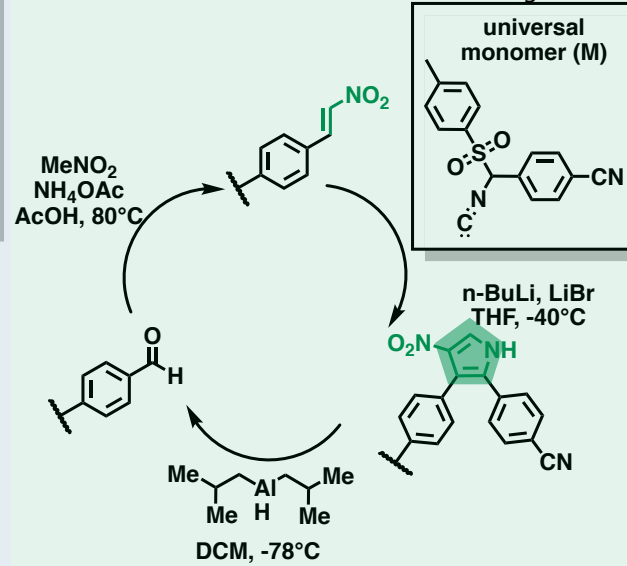
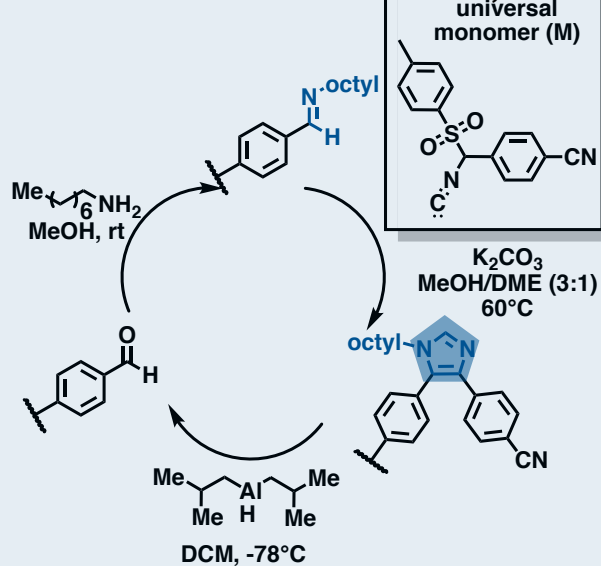
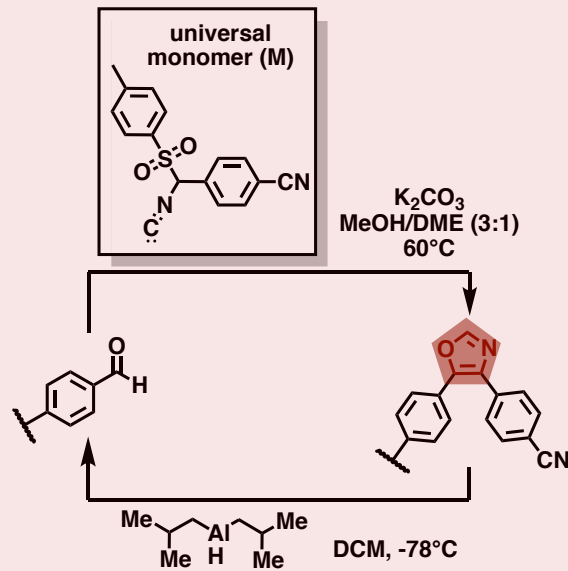
- 1
2
3 (48) Leary, E.; La Rosa, A.; González, M. T.; Rubio-Bollinger, G.; Agraït, N.; Martín, N.
4 Incorporating Single Molecules into Electrical Circuits. The Role of the Chemical
5 Anchoring Group. *Chem. Soc. Rev.* **2015**, *44* (4), 920–942.
- 6 (49) Miguel, D.; Álvarez de Cienfuegos, L.; Martín-Lasanta, A.; P. Morcillo, S.; A. Zotti, L.;
7 Leary, E.; Bürkle, M.; Asai, Y.; Jurado, R.; J. Cárdenas, D.; Rubio-Bollinger, G.; Agraït,
8 H.; Cuerva, J. M.; González, M. T. Toward Multiple Conductance Pathways with
9 Heterocycle-Based Oligo(Phenyleneethynylene) Derivatives. *J. Am. Chem. Soc.* **2015**, *137*
10 (43), 13818–13826.
- 11 (50) Kamenetska, M.; Koentopp, M.; Whalley, A. C.; Park, Y. S.; Steigerwald, M. L.;
12 Nuckolls, C.; Hybertsen, M. S.; Venkataraman, L. Formation and Evolution of Single-
13 Molecule Junctions. *Phys. Rev. Lett.* **2009**, *102* (12), 126803.
- 14 (51) T. Kim, N.; Li, H.; Venkataraman, L.; L. Leighton, J. High-Conductance Pathways in
15 Ring-Strained Disilanes by Way of Direct σ -Si–Si to Au Coordination. *J. Am. Chem. Soc.*
16 **2016**, *138* (36), 11505–11508.
- 17 (52) Cai, Z.; Zhang, N.; Awais, M. A.; Filatov, A. S.; Yu, L. Synthesis of Alternating Donor–
18 Acceptor Ladder-Type Molecules and Investigation of Their Multiple Charge-Transfer
19 Pathways. *Angew. Chemie Int. Ed.* **2018**, *57* (22), 6442–6448.
- 20 (53) Su, T. A.; Li, H.; Steigerwald, M. L.; Venkataraman, L.; Nuckolls, C. Stereoelectronic
21 Switching in Single-Molecule Junctions. *Nat. Chem.* **2015**, *7*, 215.
- 22 (54) A. Su, T.; Li, H.; Zhang, V.; Neupane, M.; Batra, A.; S. Klausen, R.; Kumar, B.; L.
23 Steigerwald, M.; Venkataraman, L.; Nuckolls, C. Single-Molecule Conductance in
24 Atomically Precise Germanium Wires. *J. Am. Chem. Soc.* **2015**, *137* (38), 12400–12405.
- 25 (55) Catalán, J.; Elguero, J. Basicity of Azoles. IV. Empirical Relationships between Basicity
26 and Ionization Potential for Aromatic Five Membered Rings Containing Nitrogen or
27 Oxygen. *J. Heterocycl. Chem.* **1984**, *21* (1), 269–270.
- 28
29
30
31
32
33
34
35
36
37
38
39
40
41
42
43
44
45
46
47
48
49
50
51
52
53
54
55
56
57
58
59
60

TOC Graphic

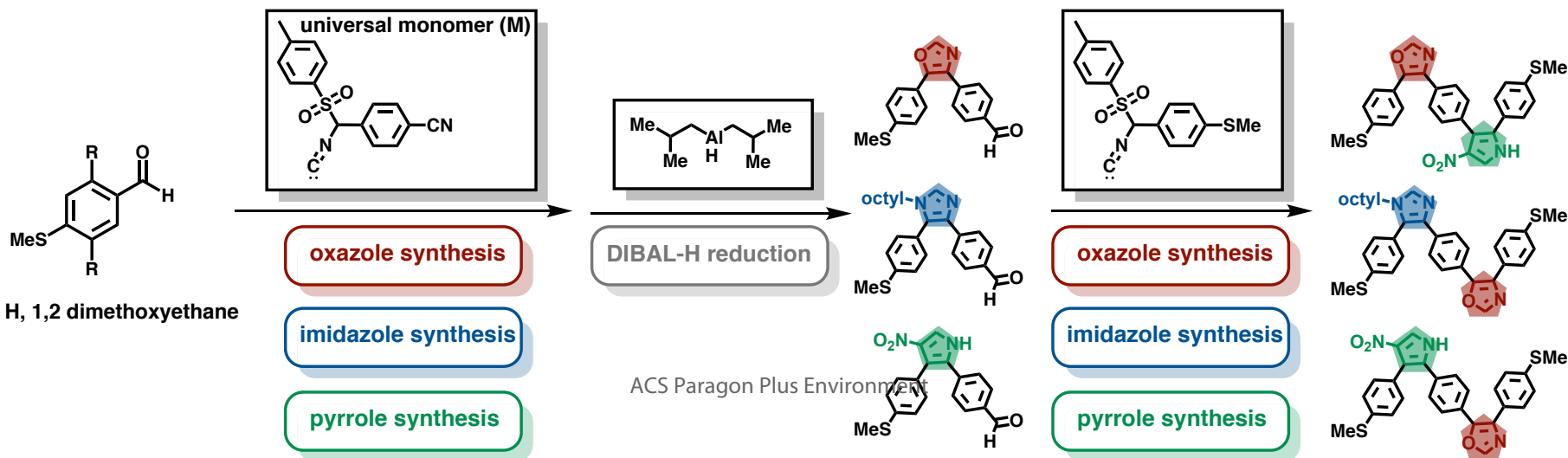


1
2
3
4
5
6
7
8
9
10
11
12
13
14
15
16
17
18
19
20
21
22
23
24
25
26
27
28
29
30
31
32
33
34
35
36
37
38
39
40
41
42
43
44
45
46
47
48
49
50
51
52
53
54
55
56
57
58
59
60

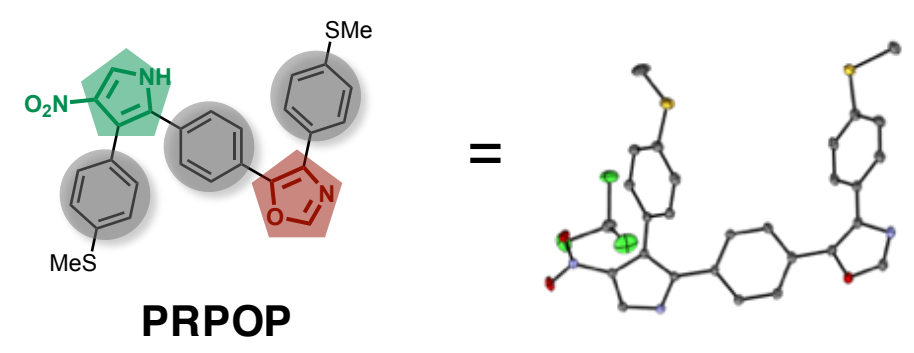
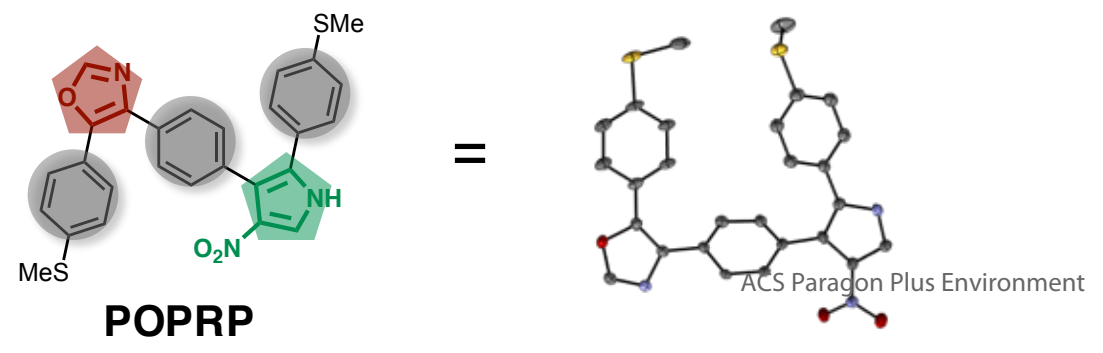
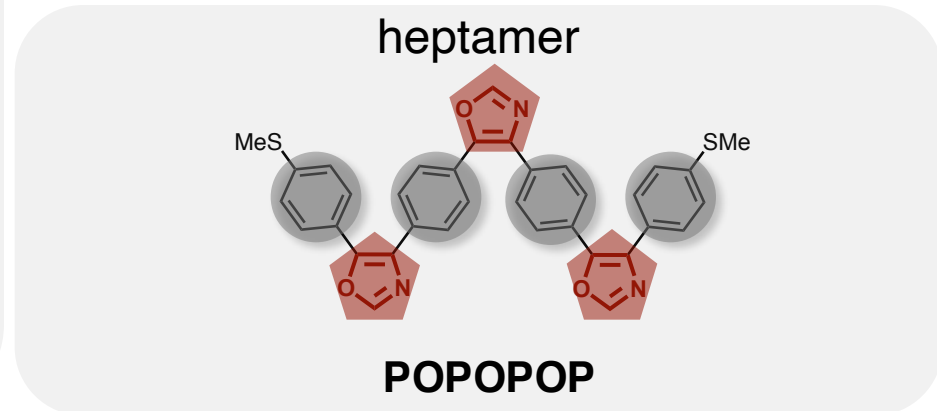
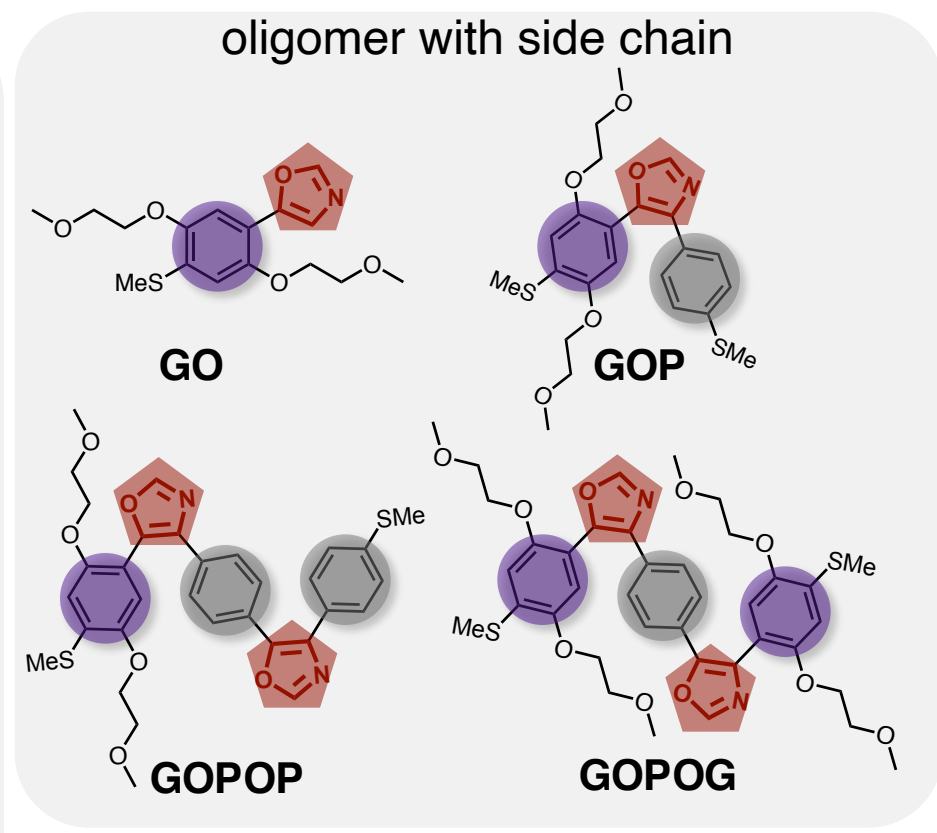
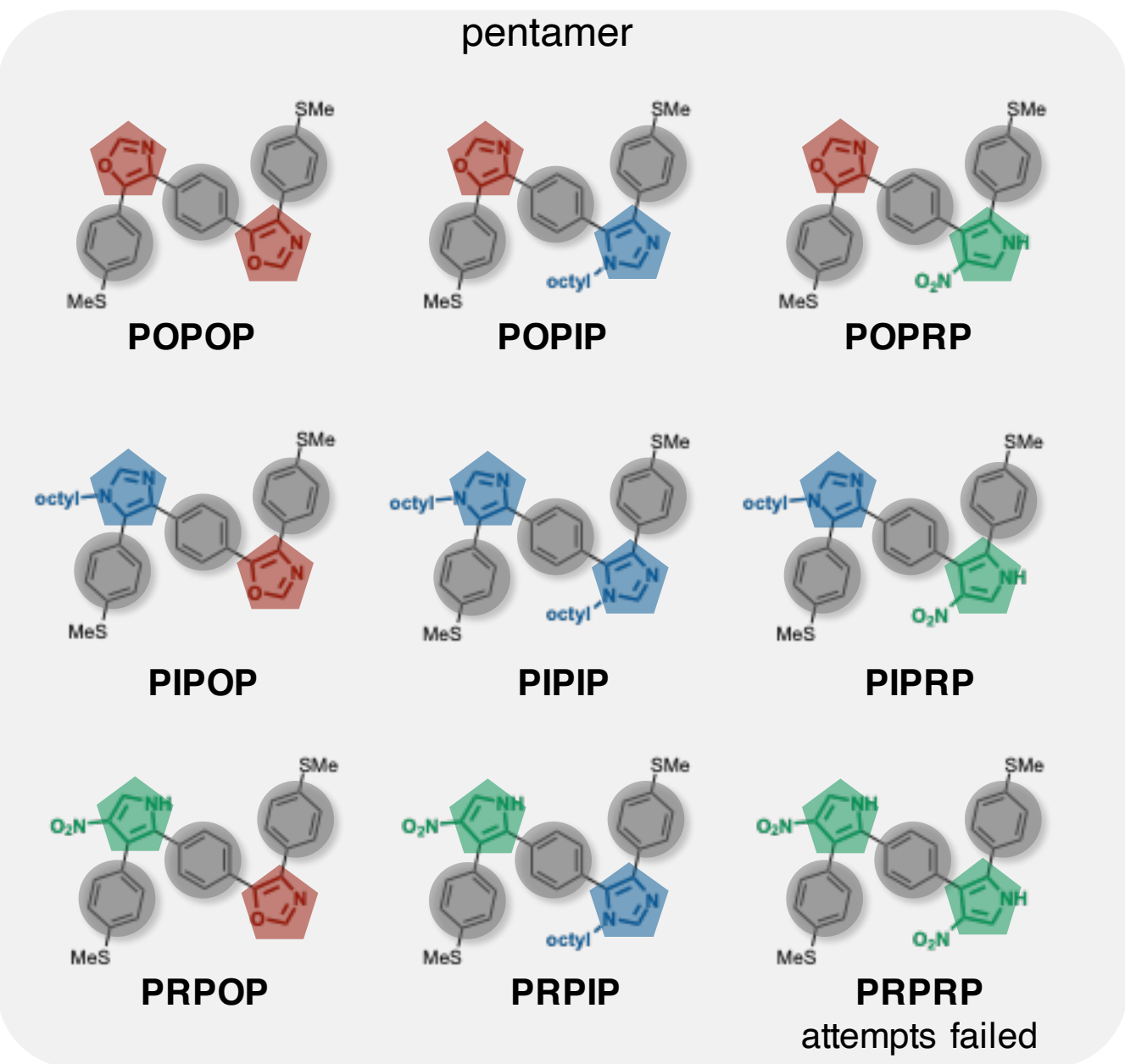
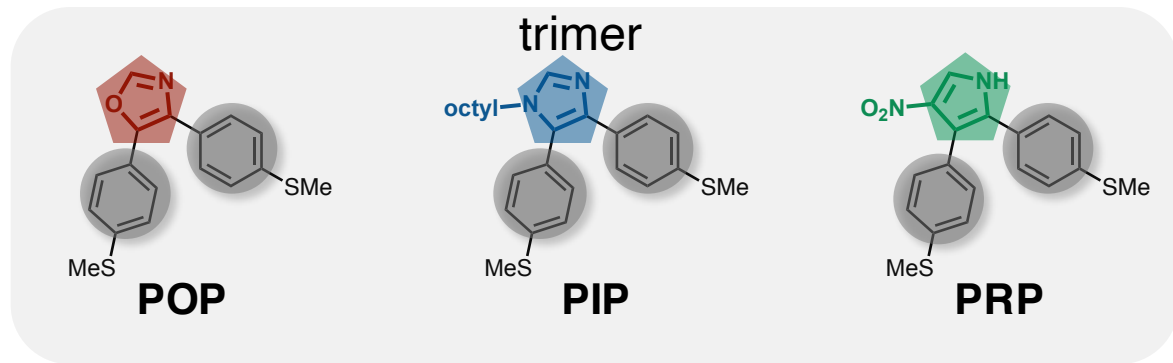
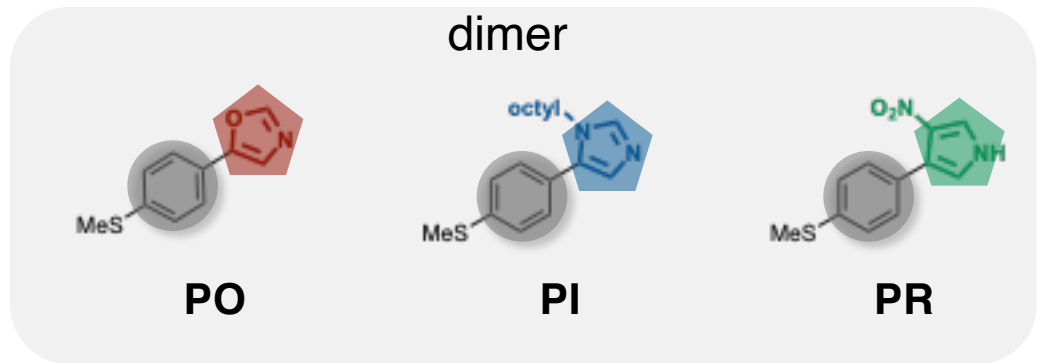
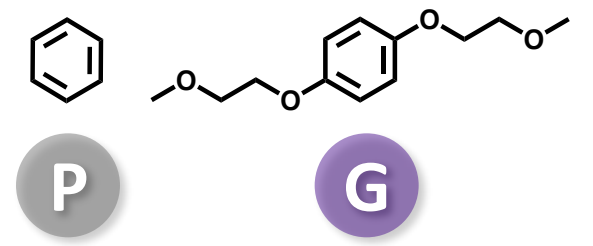
a



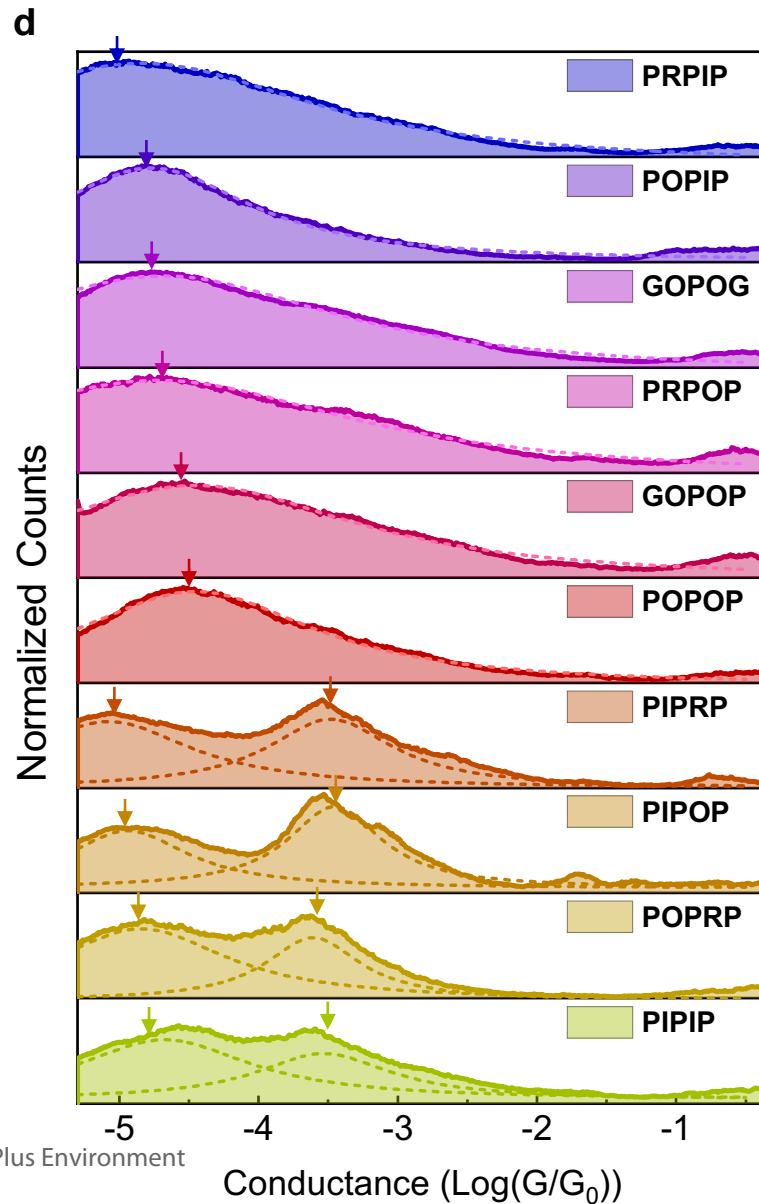
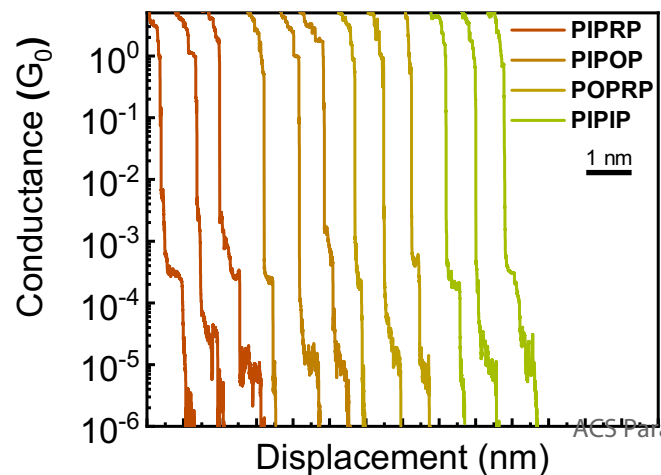
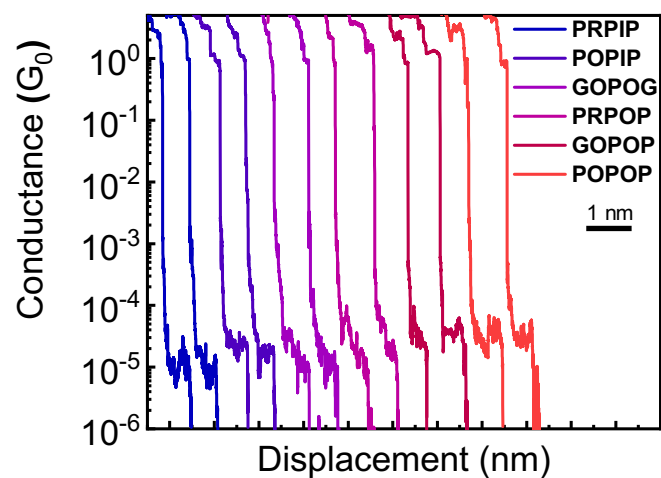
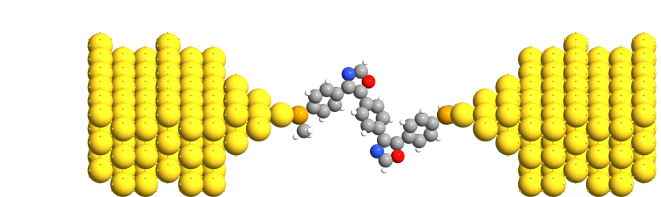
b



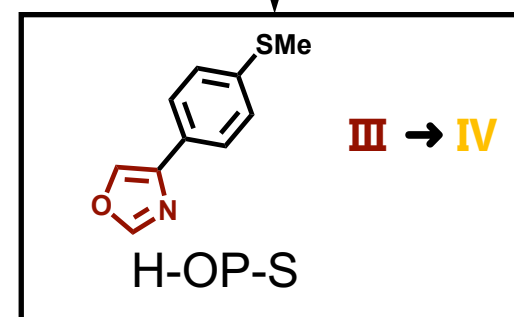
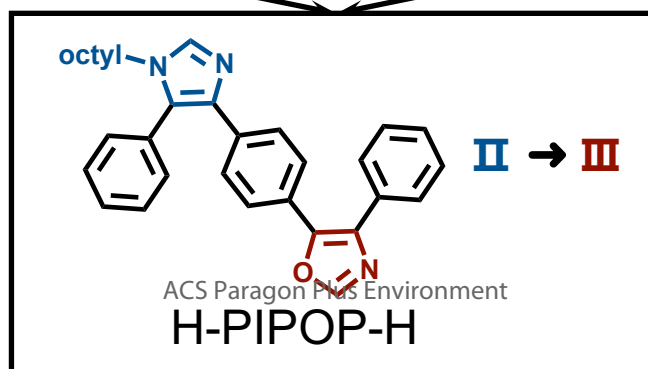
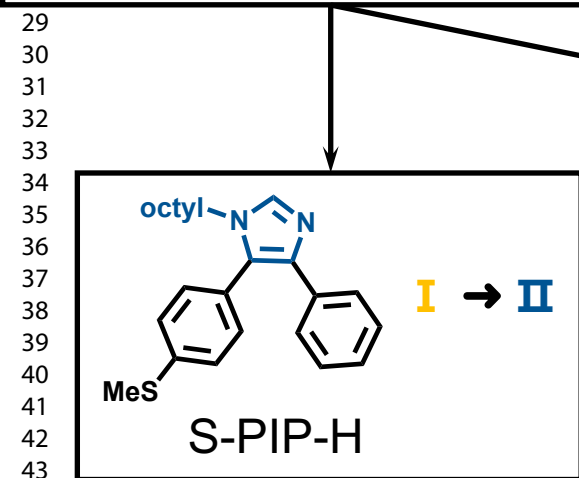
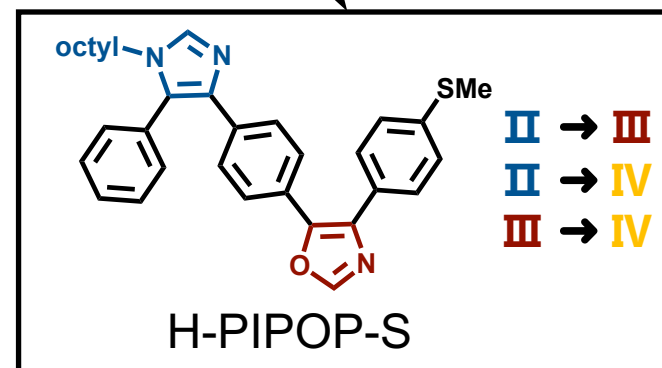
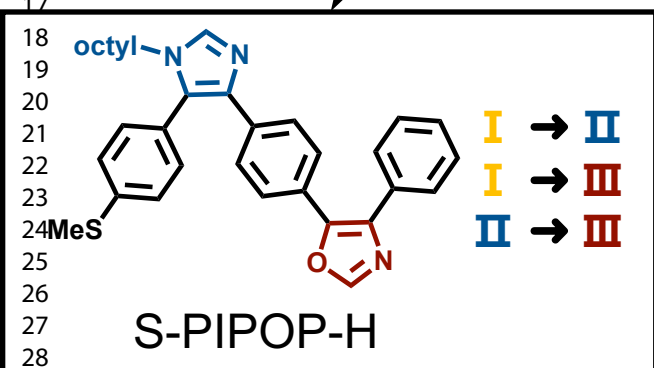
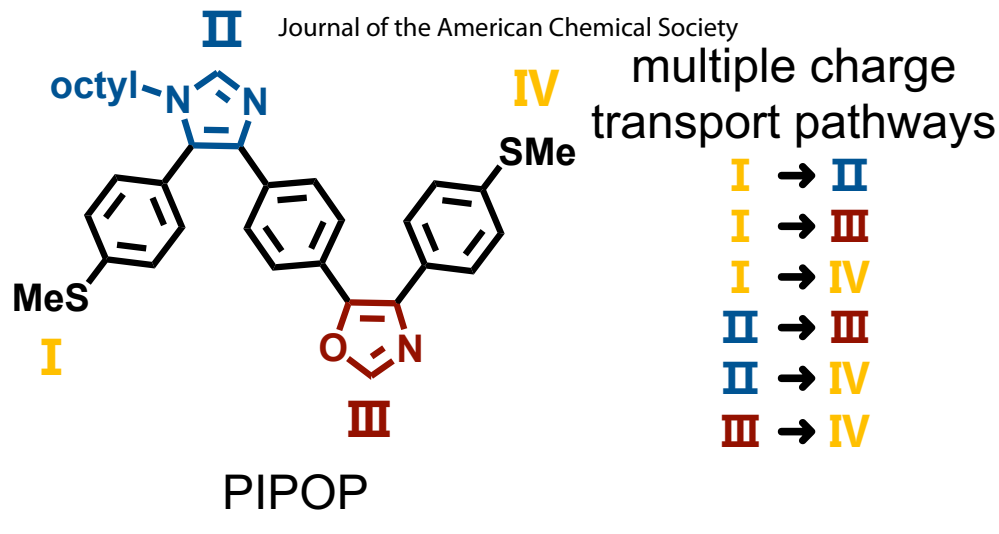
sequence definition



1
2
3
4
5
6
7
8
9
10
11
12
13
14
15
16
17
18
19
20
21
22
23
24
25
26
27
28
29
30
31
32
33
34
35
36
37
38
39
40
41
42
43
44
45
46
47
48
49
50
51
52
53
54
55
56
57
58
59
60



multiple charge transport pathways



1
2
3
4
5
6
7
8
9
10
11
12
13
14
15
16
17
18
19
20
21
22
23
24
25
26
27
28
29
30
31
32
33
34
35
36
37
38
39
40
41
42
43
44

